Acta Pharmaceutica Sinica B 2025;15(11):5867−5879

Chinese Pharmaceutical Association
Institute of Materia Medica, Chinese Academy of Medical Sciences

Acta Pharmaceutica Sinica B

www.elsevier.com/locate/apsb
www.sciencedirect.com

ORIGINAL ARTICLE

A small-molecule anti-cancer drug for long-acting lysosomal damage

Shulin Zhao[a,†], Qingjie Bai[a,†], Guimin Xue[c], Juan Wang[b], Luyao Hu[e], Xueqian Wang[a], Yan Li[a], Shuai Lu[d], Yangang Sun[b], Zhiqiang Zhang[b,*], Yanling Mu[a,*], Yanle Zhi[b,*], Qixin Chen[a,f]

[a]*School of Pharmaceutical Sciences & Institute of Materia Medica, National Key Laboratory of Advanced Drug Delivery System, Key Laboratory for Biotechnology Drugs of National Health Commission, Shandong First Medical University & Shandong Academy of Medical Sciences, Jinan 250117, China*
[b]*Engineering Technology Research Center of TCM Health Industry in Henan Province, Academy of Chinese Medical Sciences, Henan University of Chinese Medicine, Zhengzhou 450046, China*
[c]*School of Pharmacy, Henan University of Chinese Medicine, Zhengzhou 450046, China*
[d]*School of Science, China Pharmaceutical University, Nanjing 211198, China*
[e]*Tianjin University of Traditional Chinese Medicine, Tianjin 301617, China*
[f]*Departments of Diagnostic Radiology, Surgery, Chemical and Biomolecular Engineering, and Biomedical Engineering, Yong Loo Lin School of Medicine and College of Design and Engineering, National University of Singapore, Kent Ridge 119074, Singapore*

Received 3 January 2025; received in revised form 4 April 2025; accepted 9 June 2025

KEY WORDS

Lysosomal;
Anticancer;
Sub-cellular;
Small-molecule;
LLAD;
SLC38A9;
Fluorescence imaging

Abstract Lysosomes represent a promising target for cancer therapy and reducing drug resistance. However, the short treatment time and low efficiency of lysosomal targeting have limited the application in lysosome-targeting anticancer drugs. In this study, we proposed an adhesive-bandage approach and synthesized a new lysosomal targeting drug, namely long-term lysosome-targeting anticancer drug (LLAD). It contains a SLC38A9-targeting covalently bound moiety and an alkaline component both to prolong the inhibition of SLC38A9 in lysosomes and alkalinize lysosomes. Upon short term and low-dose treatment of HeLa cells, at passage 0, with LLAD, it rapidly alkalinized lysosomes and also can be detected in lysosomes even at passage 15. LLAD induced apoptosis in HeLa cells through long-term lysosomal damage, and showed better long-term anticancer effect than cisplatin *in vivo*. Overall, our study paves the way for developing long-term lysosomal targeting drugs to treat cancer and overcome the drug resistance of cancer cells, and also provides a candidate drug, LLAD, for treating cancer.

*Corresponding authors.
E-mail addresses: zhiqiangzhang2022@hactcm.edu.cn (Zhiqiang Zhang), muyanling@sdfmu.edu.cn (Yanling Mu), zhiy_1@hactcm.edu.cn (Yanle Zhi).
[†]These authors made equal contributions to this work.
Peer review under the responsibility of Chinese Pharmaceutical Association and Institute of Materia Medica, Chinese Academy of Medical Sciences.

https://doi.org/10.1016/j.apsb.2025.09.005

1. Introduction

Lysosomes are among the most important organelles in eukaryotic cells[1], housing an acidic environment and responsible for the degradation of various biological molecules[2-4]. Many lysosomal proteins are required to maintain cellular metabolism, including a lysosomal membrane-resident amino acid (especially arginine) transporter, namely solute carrier family 38 member 9 (SLC38A9)[5-7]. Aside from their traditional role as "housekeeping" organelles, lysosomes play crucial roles in the intracellular delivery of anticancer drugs[4,8]. However, lysosomes may contribute to the development of drug resistance by blocking and degrading chemotherapeutic drugs within these compartments, thereby reducing drug efficacy[9-11]. Cancer cells typically exhibit an increased number and capacity in lysosomes[12,13], but it comes with a trade-off: a less stable lysosomal membrane, which makes these cells more vulnerable to lysosome-dependent cell death[14,15]. The findings of these studies collectively highlight that lysosomes represent a promising therapeutic target for anticancer strategies[16], offering potential pathways to overcome drug resistance and improve treatment outcomes.

Numerous strategies have been proposed and used in the design of lysosome-targeting drugs for cancer therapy[17-23]. While several lysosome-targeting agents have shown efficacy in preclinical and clinical trials, significant challenges remain in designing long-term effective small-molecule drugs for this purpose[24-26]. The complexity of lysosomal functions, the harsh acidic environment and proteolytic enzymes within lysosomes render many molecules unstable and affect lysosomal escape efficiency, increasing dosing frequency and diminishing treatment efficacy[27,28]. Thus, the current arsenal of lysosome-specific targeted drugs is small. Moreover, the complementary effects, rapid lysosomal stress response (LSR) and NADH-driven lysosomal respiration may weaken the therapy effect[29]. Many listed lysosome-targeting drugs, such as chloroquine (CQ) and hydroxychloroquine (HCQ), have low anticancer activity, which limits their application[30]. As a result, the current repertoire of effective long-term lysosome-targeting drugs remains limited, underscoring the need for innovative solutions to overcome these challenges.

In this study, we proposed an adhesive-bandage approach for designing a long-acting lysosome-targeting anticancer drug. We used this approach, which combines an SLC38A9-targeting covalently bound moiety and an alkaline component to prolong the inhibition of SLC38A9 and alkalinize lysosomes, to design and synthesize the novel potential anticancer drug long-term lysosome-targeting anticancer drug (LLAD). Remarkably, LLAD also exhibits intrinsic fluorescence properties, which enable precise monitoring of the localization and activity of the compound within cancer cells while providing insights into the lysosomal status. LLAD was first confirmed to specifically interact with SLC38A9 in lysosomes. Due to its characteristics, LLAD showed excellent long-term lysosomal retention in HeLa cells even after 15 passages, and effectively alkalinize lysosomes. Additionally, we also investigated the anticancer mechanisms of action of LLAD, and found that it induced apoptosis in HeLa cells through long-term lysosomal damage. *In vivo*, LLAD also showed an excellent long-term anticancer effect in BALB/c mice (Fig. 1). In summary, LLAD overcomes the limitations of conventional lysosome-targeting drugs, thus providing a novel lysosome-targeting drug and a new perspective to design lysosome-targeting drugs.

2. Results and discussion

2.1. Design and characterization of LLAD

In this study, to develop long-term lysosome-targeting drugs, we proposed an adhesive-bandage approach, which involves two key components: i) an SLC38A9-targeting covalently bound moiety to prolong the interaction with the target and bind with SLC38A9[31,32]; ii) an alkaline component to alkalinize lysosomes (Fig. 1). To implement this approach, we first determined that the Cys363 amino acid residue of SLC38A9 is located in its arginine binding site, which can thus be used to design irreversible inhibitors. Molecular docking showed that 3-(1*H*-benzol-2-yl)-1*H*-indazole binds to SLC38A9 and occupies the arginine binding pocket. Indazole formed two hydrogen bonds with Thr121 and the amide formed one hydrogen bond with Thr117. On one side, the benzene ring of indazole extends to Cys363 and acrylamide group was introduced to the benzene ring. The distance from the acrylamide to Cys363 is 4.63 Å, and this is prone to form a covalent bond with Cys363 (Supporting Information Fig. S1). On the other side, the benzene ring of benzimidazole extends outward from the binding pocket, and the introduction of the alkaline compound here is also beneficial for enhancing the binding to SLC38A9. Furthermore, we incorporated *N*-methyl piperazine into the molecule, which can be used to alkalinize lysosomes[33]. Based on this approach, we obtained compound LLAD (Fig. 2A). The best conformation of the SLC38A9−LLAD complex obtained by covalent docking analysis was then used as the initial conformation for molecular dynamics simulation. The simulation results revealed that the acrylamide group in the molecule forms covalent bonds with Cys363, as well as stable hydrogen bonds with Asn362 (Fig. 2B). In addition, the entire system approaches equilibrium after 50 ns, the backbone root-mean square maintains stability at around 4.6 Å for the receptor and at around 1 Å for the ligand during the entire simulation (Fig. 2C), indicating the high stability of the SLC38A9−LLAD complex.

After its synthesis (Supporting Information Fig. S2), LLAD was characterized by proton nuclear magnetic resonance (^{1}H NMR) spectroscopy, carbon-13 NMR (^{13}C NMR) and high-resolution mass spectrometry (HRMS) (Supporting Informations Figs. S3−S9). We tested its anti-proliferation activity against cancer cells, the IC_{50} was approximately 0.2168 μmol/L in HeLa cells, 26.66 μmol/L in A549 cells and 2.478 μmol/L in HL-60 cells (Supporting Information Fig. S10) after treated by LLAD for 48 h. And the IC_{50} of LLAD treated on HeLa cells for 24 h was 1.049 μmol/L. The results indicated that HeLa cervical cancer cells are significantly more sensitive to LLAD than the other tested cell lines, and the cytotoxicity

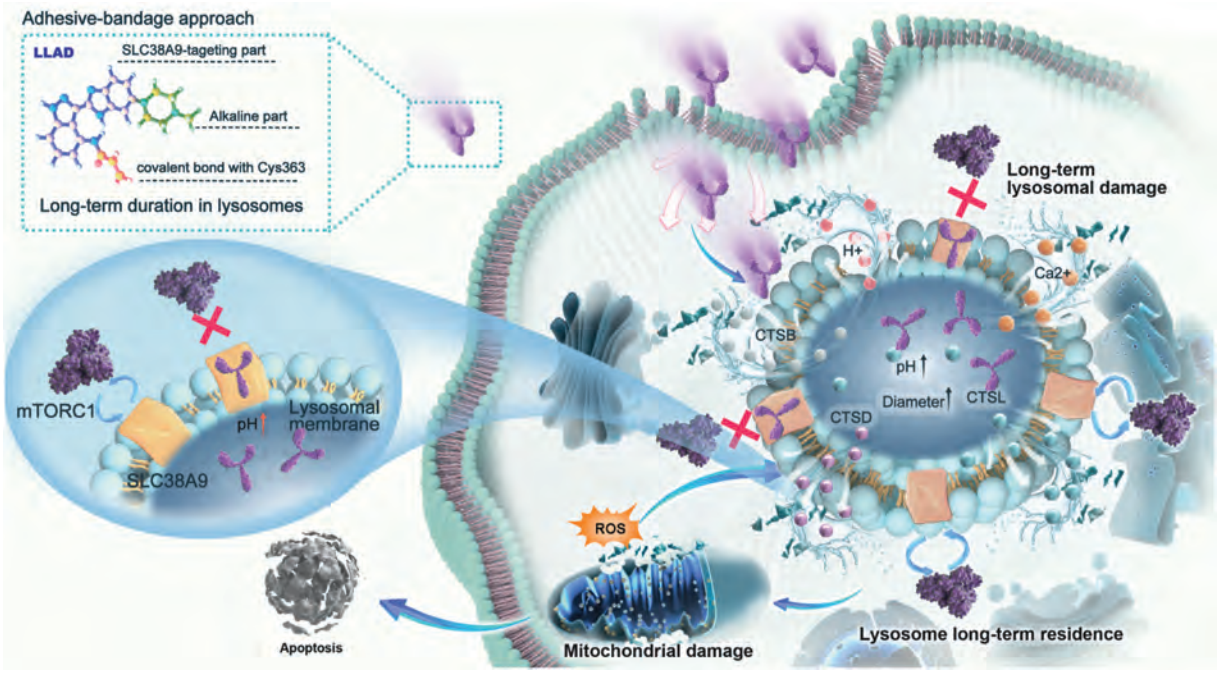

Figure 1 Schematic diagram of the approach to design an anticancer drug for long-acting lysosomal damage. To develop an anticancer drug for long-term activity and lysosomal damage, we proposed a novel strategy "adhesive-bandage approach", including an SLC38A9-targeting covalently bound moiety and an alkaline component to prolong the retention and to alkalinize lysosomes. Using this approach, we designed an anticancer drug, and termed long-term lysosome-targeting anticancer drug (LLAD). We confirmed that LLAD prolonged the retention in lysosomes and alkalization of lysosomes. It also induced mitochondrial apoptosis in HeLa cells through long-term lysosomal damage.

was dose-dependent (Supporting Information Figs. S10 and S11). To confirm the binding of LLAD to SLC38A9, the surface plasmon resonance (SPR) qualification analysis revealed that LLAD binding with SLC38A9 and the K_D value reached 1.29 μmol/L (Fig. 2D). We also performed a cellular thermal shift assay (CETSA), and the result of the CETSA revealed that the thermotolerance of LLAD-treated SLC38A9 protein was significantly increased[34,35] (Fig. 2E). Given that SLC38A9 regulates the activity of rapamycin complex 1 (mTORC1)[5,36], we tested the effect of LLAD to the mTOR signaling pathway. The result indicated that the phosphorylation of mTOR and the substrates S6 kinase (S6K) were inhibited by LLAD (Fig. 2F−H). Thus, we confirmed that LLAD can directly inhibit the activity of SLC38A9. Furthermore, LLAD also exhibited fluorescence properties, with optimal excitation wavelength and emission wavelength of 405 and 470 nm, respectively (Supporting Information Fig. S12). Confocal fluorescence microscopy images of LLAD showed that it predominantly localized in HeLa cells in a short time (Supporting Information Fig. S13). To verify that LLAD directly interacts with lysosomes, the commercial lysosomal probe Lyso-tracker Red (LTR) was used in localization experiments. As expected, the Pearson's colocalization coefficient (PCC) of LLAD and LTR was significantly higher than that of other organelles, indicating that LLAD specifically interacted with lysosomes (Fig. 2I−K, Supporting Information Fig. S14), and the fluorescence signal of LLAD was not affected by acidic conditions (Supporting Information Fig. S15). These findings validate our hypothesis that LLAD specifically localizes to lysosomes. Collectively, LLAD was a novel lysosome-targeting drug through binding with SLC38A9 and its alkaline (Fig. 2L).

2.2. *Long-acting in the lysosomes and alkalinisation of the lysosomes by LLAD in the lysosomes*

Long-acting *in vivo* is particularly important for cancer treatment[37]. We evaluated the duration of the retention of LLAD within lysosomes, by first evaluating its colocalization with LTR after treatment for different time periods. At the same cell passage, the PCC values remained constant even after 72 h of treatment, indicating sustained lysosomal localization of LLAD (Supporting Information Fig. S16). We then investigated the behavior of LLAD across multiple cell passages using Lyso-Tracker Deep Red (LTDR) as a control. The LTDR, a commercial lysosomal pH-dependent fluorescent probe that can be protonated and sequestered in lysosomes for a long time, was used in this experiment as a control. The confocal fluorescence microscopy images of HeLa cells, taken from passages 0 to 15 after treatment with LLAD (1 μmol/L, 24 h) and LTDR (100 nmol/L, 24 h) are shown in Fig. 3A and B, and Supporting Information Fig. S17. Notably, with increasing cell passage, the fluorescence intensity of LTDR decreased dramatically, ultimately vanishing at passage 5 (Fig. 3B). In contrast, the fluorescence intensity of LLAD persisted through passage 15, indicating that LLAD exhibits a longer duration in lysosomes compared to LTDR (Fig. 3B and C).

In addition to prolonged retention, alkalinize lysosomes is another key goal we aimed to achieve. The proper function of lysosomes is highly contingent upon their acidic internal pH[38]. In this context, the methyl piperazine structure plays a critical role in the alkalization of lysosomes and the alkaline environment is more beneficial to the intake of acidic amino acids. Additionally, the accumulation of acidic amino acids can inhibit the activity of

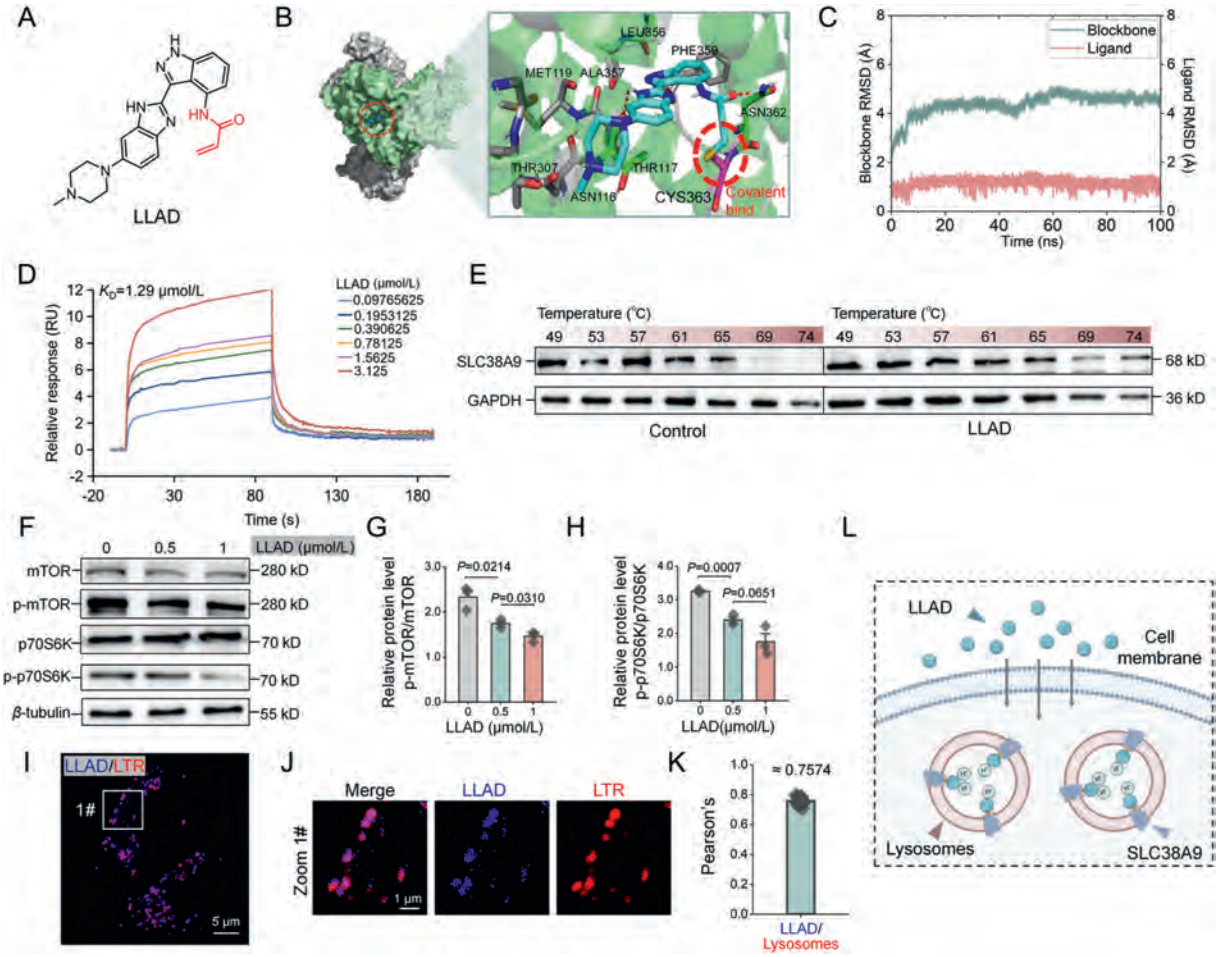

Figure 2 Design and characterization of LLAD. (A) Chemical structure of LLAD compound. (B) Representative binding modes of LLAD with SLC38A9 from the equilibrium period of the molecular dynamics run; The binding mode of LLAD with SLC38A9 was visualized by PyMOL, hydrogen bonds are shown with red dotted lines and the red dotted circle represents the covalent bond. (C) Average root mean square deviation (RMSD) of backbone atoms of the SLC38A9 protein and compound LLAD during the MD simulation. (D) LLAD exhibited a potent binding ability with SLC38A9 determined by an SPR assay. (E) LLAD promoted the resistance of SLC38A9 to different temperature gradients by CETSA in HeLa cells. (F) Western blot analysis to detect mTOR, p-mTOR, p70S6K and p-p70S6K protein expression in HeLa cells. Three independent biological replicates were performed, and the results were similar. (G) Quantitative analysis of p-mTOR/mTOR protein changes in HeLa cells incubated with LLAD by different concentrations (n = 3). (H) Quantitative analysis of p-p70S6K/p70S6K protein changes in HeLa cells incubated with LLAD by different concentrations (n = 3). (I) Confocal fluorescence microscopy images of LLAD (10 μmol/L, 2 h) and LTR (100 nmol/L, 30 min) in HeLa cells. (J) Zoomed-in images correspond to the white rectangles #1 in Fig. 2I. (K) Data analysis of the colocalization of LLAD and LTR; data are presented as the mean ± SD (n = 15 areas). (L) Schematic diagram of LLAD interacting with lysosomes, suggesting that LLAD targets lysosomes through interaction with SLC38A9 and the acid environment in lysosomes. LLAD channel: λ_{ex} = 405 nm, Em_{max} = 470 nm (411−500 nm); LTR channel: λ_{ex} = 561 nm, Em_{max} = 577 nm (570−694 nm); the analysis of the different groups was performed using two-tailed unpaired Student's t-test, and the data are presented as the mean ± SD. A value of $P < 0.05$ was considered statistically significant.

V-ATPase, a proton pump that uses adenosine triphosphate (ATP) to pump protons into lysosomes[7,39], and thus a critical regulator of lysosomal pH. As shown in Fig. 3D and E, we observed a strong reduction in fluorescence intensity of the probe in lysosomes treated with low-dose LLAD compared to the control group CQ, indicating a shift toward a more alkaline lysosomal environment (Fig. 3G). This disruption in lysosomal acidity impairs enzymatic activity[40], as confirmed by the decreased activity of Cathespin D (CTSD) in LLAD-treated HeLa cells (Fig. 3F). In LLAD-treated HeLa cells, significant lysosomal clustering was evident, underscoring the ability of the drug to induce the LSR[41,42] (Fig. 3H and I).

2.3. *LLAD induced lysosomal damage by long-term retention*

We further confirmed the effects of the LLAD-induced LSR. As shown in Fig. 4A and B, the treatment with LLAD led to a significant increase in lysosomal diameter, indicating morphological alterations associated with LSR in 12 h. We assessed lysosomal membrane integrity using acridine orange (AO), a fluorescent dye commonly used to assess lysosomal membrane integrity[21]. AO was excited using identical powerful laser and lysosomal membrane disruption and leakage of AO into cytoplasm were monitored by acquiring time-lapse images for a total period of 300 s. The ratio of red to green fluorescence serves as a reliable indicator

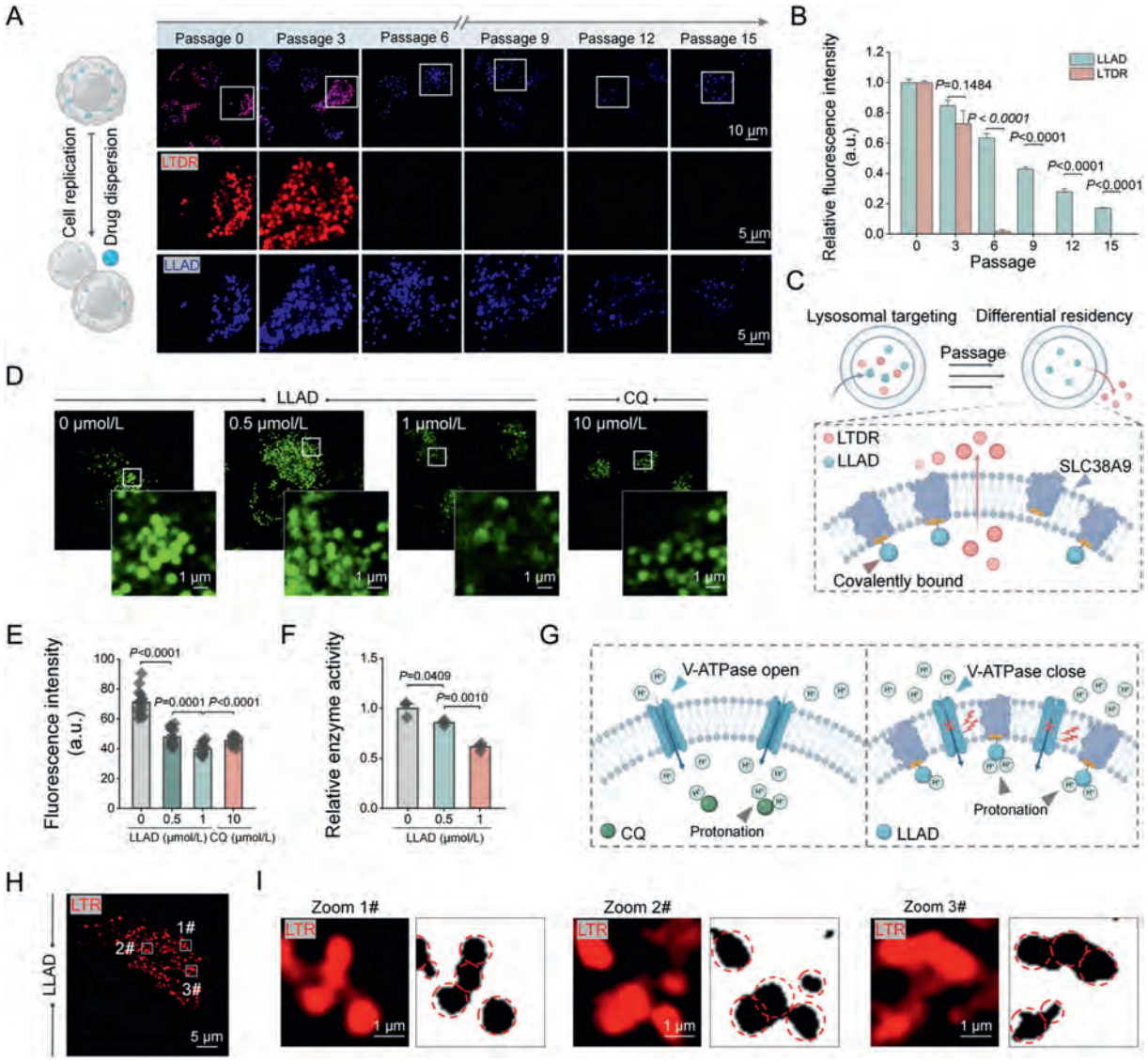

Figure 3 Long-acting in the lysosomes and alkalinisation of the lysosomes by LLAD in the lysosomes. (A) Schematic diagram and representative confocal fluorescence microscopy images of LLAD and LTDR retention in lysosomes at the different passages of HeLa cells. (B) Data analysis of the fluorescence intensity of LLAD and LTDR; data are presented as the mean ± SD ($n = 3$). (C) Schematic diagram of LLAD prolonged retention in lysosomes compared to LTDR through covalently binding with SLC38A9. (D) Representative confocal fluorescence microscopy images of Lysosensor Green DND-189 (a pH sensor) in HeLa cells, treated with LLAD (0, 0.5 and 1 μmol/L), the CQ group served as a positive group. (E) Quantitative analysis of the fluorescence intensity of Lysosensor Green DND-189 in LLAD-treated or CQ-treated HeLa cells; data are presented as the mean ± SD ($n = 15$ cells). (F) Quantitative analysis of the activity of CTSD in HeLa cells treated with LLAD for 24 h; three independent biological replicates were performed, and the results were similar. (G) Schematic diagram of LLAD-alkalinized lysosomes by inhibiting V-ATPase function and alkalinize lysosomes, while CQ treatment alkalinized lysosomes through protonation. (H) Representative structure illumination microscopy (SIM) images of lysosomes labeled with LTR in LLAD-treated (1 μmol/L, 12 h) HeLa cells. (I) Zoomed-in images correspond to the white rectangles #1, #2 and #3 in Fig. 3H. LLAD channel: $\lambda_{ex} = 405$ nm, $Em_{max} = 470$ nm (411−500 nm); LTR channel: $\lambda_{ex} = 647$ nm, $Em_{max} = 668$ nm (651−694 nm); different groups analysis was performed using two-tailed unpaired Student's *t*-test, and the data are presented as the mean ± SD. A value of $P < 0.05$ was considered statistically significant.

of lysosomal membrane integrity. Our results revealed an increase in green fluorescence and a decrease in red fluorescence, confirming that LLAD induces lysosomal membrane permeabilization (Fig. 4C−F). Remarkably, the expression of lysosomal specific membrane proteins, such as lysosomal associated membrane protein 1 (LAMP1), Cathespin B (CTSB), Cathespin D (CTSD) and Cathespin L (CTSL), were not significantly changed in LLAD-treated HeLa cells (Supporting Information Figs. S18 and S19). Thus, our findings confirm that LSR is indeed triggered by treatment with LLAD in HeLa cells, which is consistent with our initial hypothesis.

Noteworthy, LSR can lead to varied outcomes, such as lysosomal repair or damage, depending on the intensity of the inducing stimulus[29,43]. To investigate whether LLAD can induce lysosomal damage in HeLa cells after induced LSR, we used transmission electron microscope (TEM) to examine the

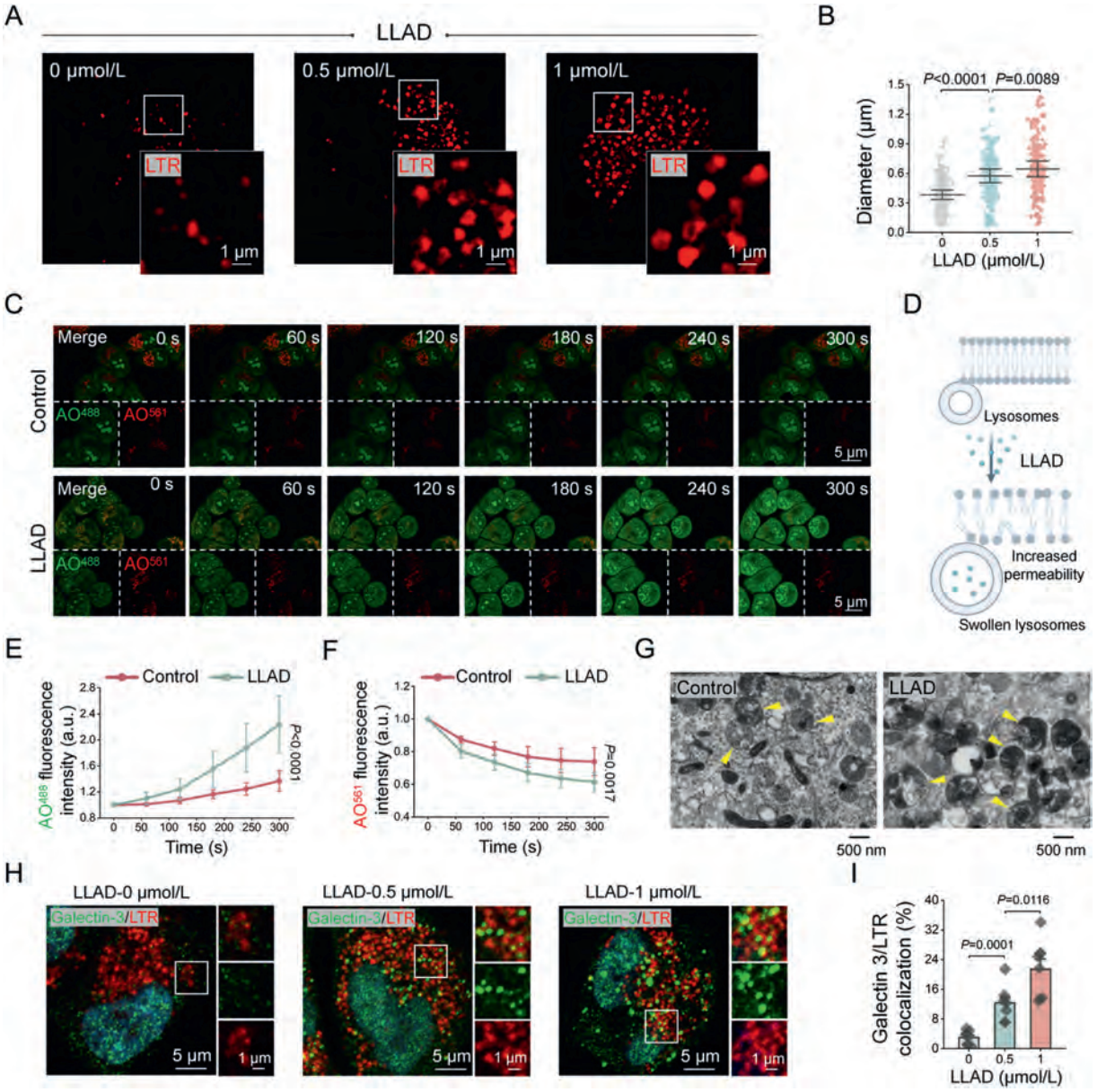

Figure 4 LLAD induced lysosomal damage by long-term retention. (A) Representative SIM images of lysosomes labeled with LTR in LLAD-treated HeLa cells, enlarged image of white rectangle in the right lower part. (B) Quantitative analysis of the diameter of lysosomes in HeLa cells treated with LLAD after 12 h; data are presented as the mean ± SD (n = 200 particles). (C) Time-dependent confocal fluorescence microscopy images of acridine orange (AO, 2.0 μg/mL) after continuous exposure to laser light in HeLa cells with or without LLAD (1 μmol/L, 12 h) treatment. (D) Schematic diagram of LLAD treatment leading to swollen lysosomes and increased permeability of lysosomes. (E) Quantitative analysis the green fluorescence of AO. (F) Quantitative analysis the red fluorescence of AO. (G) TEM images of lysosomes in LLAD-treated (1 μmol/L, 24 h) and control HeLa cells. The yellow arrows indicate lysosomes. (H) HeLa cells were treated with LLAD (1 μmol/L) for 24 h, and stained with rabbit anti-galectin 3 (green), 4′,6-diamidino-2-phenylindole (DAPI; blue) and LTR (red) observed by confocal fluorescence microscopy. Enlarged images of white rectangle in the right part. (I) Quantitative analysis of the colocalization of galectin 3 and LTR; data are presented as the mean ± SD (n = 5 cells). LTR channel: λ_{ex} = 561 nm, Em_{max} = 577 nm (570−694 nm); AO^{488} channel, λ_{ex} = 488 nm, Em_{max} = 530 nm (500−550 nm); AO^{561} channel, λ_{ex} = 561 nm, Em_{max} = 640 nm (580−694 nm). Galectin 3 channel: λ_{ex} = 488 nm, Em_{max} = 520 nm (500−550 nm). Analysis of different groups was performed using two-tailed unpaired Student's t-test, and the data are presented as the mean ± SD. A value of $P < 0.05$ was considered statistically significant.

morphology of lysosomes. The TEM analysis revealed significant lysosomal alterations, including membrane disruption, loss of integrity, and the formation of vacuolar structures within the lysosomes of LLAD-treated cells (Fig. 4G). These findings indicated that LLAD indeed caused lysosomal damage. Furthermore, the colocalization of lysosomes and galectin-3 (a marker for lysosomal damage) was significantly increased in HeLa cells treated with LLAD[44,45], reaching a ratio of 20% (Fig. 4H and I). When lysosomal damage occurs, lysosome-targeting drugs may escape from the lysosomes and undergo subsequent repair

processes, reducing their effectiveness. To explore this issue further, we investigated the behavior of these drugs under conditions of lysosomal damage induced by L-leucyl-L-leucine methyl ester hydrobromide (LLOMe). Our findings confirmed that LLAD remained in the lysosomes despite the lysosomal damage. In contrast, LTDR showed a significant reduction within the lysosomal compartments (Supporting Information Figs. S20 and S21). Taken together, our results demonstrate that the prolonged retention of LLAD in lysosomes induces LSR and leads to lysosomal damage in HeLa cells, highlighting its potent effects on targeted lysosomes.

2.4. LLAD demonstrated strong anticancer activity against HeLa cells by sustained lysosomal damage

To determine the mechanism underlying LLAD-induced cell death through long-term lysosomal damage[43,46-48], HeLa cells were pretreated with inhibitors of many known cell death mechanisms, and cisplatin was used as a positive control[49]. The results revealed that LLAD primarily induces apoptosis (Supporting Information Figs. S22 and S23). As shown in Fig. 5A and B, the decrease in mitochondrial membrane potential that occurred in HeLa cells treated with 0.5 μmol/L LLAD indicated mitochondrial damage, including swelling[50] (Supporting Information Figs. S24 and S25). Lysosomes as a component of antioxidation defense system in cells[51,52], and the failure to stop the excessive reactive oxygen species (ROS) production timely also increase the extent of lysosomal damage. Mitochondria damage also enhances ROS production[53]. The levels of ROS were significantly increased by treatment with LLAD (Supporting Information Fig. S26) and exacerbated lysosomal damage[54]. Analysis of apoptotic markers showed upregulation of Bax, Cleaved Caspase-3, and Cleaved PARP1[55-57] (Fig. 5C−E, Supporting Information Fig. S27), confirming that LLAD induced mitochondrial-dependent apoptosis. Flow cytometry analysis further supported this conclusion[58] (Fig. 5F and G). Moreover, LLAD significantly increased the concentration of intracellular Ca^{2+}, a key regulator of lysosomal function and apoptosis (Supporting Information Fig. S28).

To determine the link between lysosomal damage and mitochondria-dependent apoptosis, we investigated the lysosomal−mitochondrial axis[59]. Colocalization of galectin 3 with LTR confirmed lysosomal damage at low LLAD doses (0.1 μmol/L) (Supporting Information Fig. S29). However, mitochondrial changes occurred at 0.5 μmol/L (Supporting Information Figs. S30 and S31). These results support that LLAD-induced mitochondrial dysfunction and apoptosis are mediated through lysosomal damage. Lysosomal dysfunction and apoptosis also influence cancer cell invasion and migration. Wound healing assays showed that LLAD significantly inhibited HeLa cell migration (Supporting Information Fig. S32). Additionally, Transwell assays further demonstrated that LLAD inhibited cell invasion in a dose-dependent manner[60] (Fig. 5H and I). In summary, LLAD induces apoptosis *via* the lysosomal−mitochondrial axis and effectively inhibits HeLa cell migration and invasion, underscoring its potential as a targeted anticancer agent.

2.5. LLAD exhibited excellent long-term anticancer effect in vivo

Given the promising anticancer activity of LLAD *in vitro*, we evaluated its potential *in vivo* using a HeLa xenograft mouse model. LLAD was administered orally once daily for 21 days after tumors reached approximately 100 mm^3 in volume. Tumor volume and body weight were measured every three days (Supporting Information Fig. S33). Noteworthy, there were no significant changes in body weight across treatment groups (Supporting Information Fig. S34A). However, tumor volume decreased significantly by Day 13 in LLAD-treated mice (Supporting Information Fig. S35A), and tumor weight in LLAD-treated mice was reduced in a dose-dependent manner compared to controls (Supporting Information Fig. S35B and S35C). Initial analysis demonstrated significant tumor accumulation of LLAD (Fig. 6B). Histological analysis revealed extensive apoptosis in LLAD-treated tumors (Supporting Information Fig. S36), and immunohistochemistry analysis confirmed increased levels of Bax, Cleaved Caspase-3 and Cleaved PARP1 although this effect was dose-dependent (Supporting Information Fig. S37). The histological analysis of tissues from animals treated with different condition had no significant changes in each group, which revealed that LLAD was safe *in vivo* in work concentration (Supporting Information Fig. S38).

To verify the long-time antitumor activity of LLAD *in vivo*, liquid chromatography-mass spectrometry (LC−MS) was used to measure the level of LLAD in tumor tissue. The results showed that LLAD persisted longer in tumors compared to the positive control (Supporting Information Fig. S39). In addition, the same concentration of LLAD and cisplatin, whose efficiency was confirmed not to change significantly by oral administration once a day, was orally administered once every three days until Day 30 (Fig. 6A). The body weight of the mice was not significantly changed (Fig. S34B). As shown in Fig. 6C−E, the tumor in the positive group was not significantly different from the normal group, and LLAD-treated tumors were still smaller than those in other groups, which indicated its long-term antitumor effect. As shown in Fig. 6F−I, LLAD treatment effectively induced apoptosis in tumor tissue, while cisplatin showed minimal inhibitory effects on tumor growth. The result of TEM also exhibited that lysosomal damage in LLAD-treated tumor tissue (Fig. 6J). These findings underscore the potent and sustained antitumor effects of LLAD, supporting its potential as a promising anticancer therapeutic agent.

3. Conclusions

In this study, we proposed an "adhesive-bandage approach" and successfully synthesized a fluorescent small-molecule lysosome-targeteding drug, namely LLAD. It specifically accumulates in lysosomes through lysosomal uptake, where it covalently binds to SLC38A9 and alkalinity. Antiproliferation assays demonstrated that HeLa cells were more sensitive to LLAD compared to other cell lines. The results of molecular docking analysis, molecular dynamics simulation, SPR, CETSA and Western blot analysis confirmed that LLAD targets SLC38A9, while confocal fluorescence microscopy imaging revealed its long-term retention in lysosomes. Further investigations showed that LLAD induced sustained lysosomal damage and apoptosis in HeLa cells, and also inhibited their invasion and migration abilities. *In vivo*, LLAD exhibited significant antitumor activity in a dose-dependent manner. Even at equivalent doses, LLAD outperformed positive controls such as cisplatin, demonstrating superior efficacy and more prolonged activity. These findings confirm LLAD as a high-performance lysosome-targeting drug delivery with both *in vitro* and *in vivo* anticancer effects.

Importantly, we also established LLAD as a small-molecule anticancer drug with a long retention in lysosomes. Compared

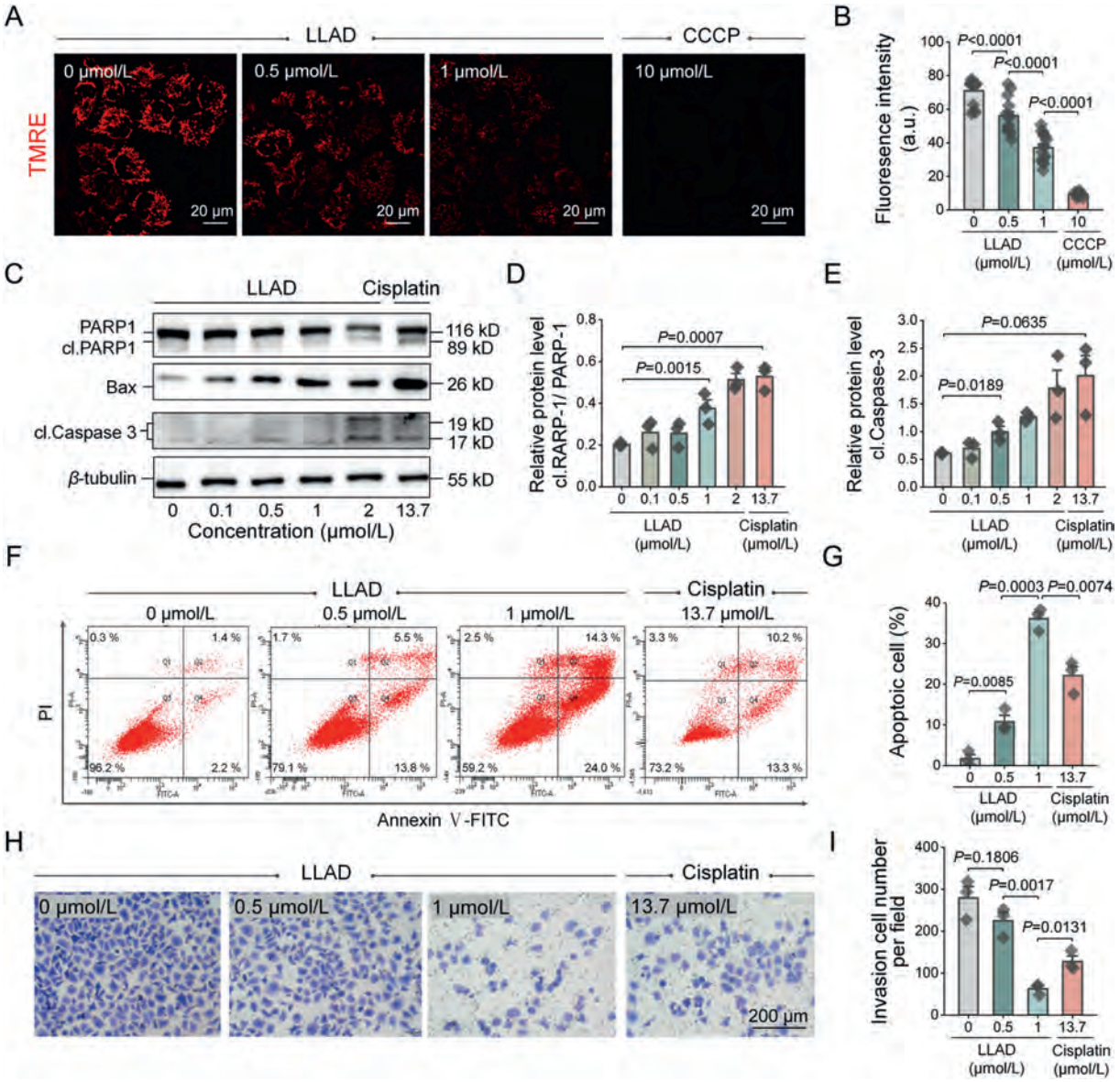

Figure 5 LLAD demonstrated strong anticancer activity against HeLa cells by sustained lysosomal damage. (A) Representative confocal fluorescence microscopy images of tetramethylrhodamine, ethyl ester (TMRE) in the HeLa cells at different concentrations of LLAD for 24 h. Carbonyl cyanide 3-chlorophenylhydrazone (CCCP; 10 μmol/L, 1 h) group was used as a positive group. (B) Quantitative analysis of the fluorescence intensity of TMRE in HeLa cells treated with LLAD. Data are presented as the mean ± SD (n = 15 cells). (C) Western blot analysis to detect the expression of protein associated with apoptosis in HeLa cells treated with LLAD (0, 0.1, 0.5, 1 and 2 μmol/L) or cisplatin (13.7 μmol/L) for 24 h. Three independent biological replicates were performed, and the results were similar. (D) Quantitative analysis of expression of cleaved PARP1/PARP1 in HeLa cells treated by LLAD. Data are mean ± SD (n = 3). (E) Quantitative analysis of expression of cleaved caspase-3 in HeLa cells treated by LLAD. Data are mean ± SD (n = 3). (F) Cell apoptosis in HeLa cells affected by different concentrations of LLAD through flow cytometry using an Annexin V-FITC Apoptosis Detection Kit, cisplatin group as positive group. (G) Quantitative analysis of percentage of Q2 and Q4 in flow cytometry HeLa cells treated by LLAD. Data are mean ± SD (n = 3). (H, I) Representative images and quantitative analysis the number of invasion cells showing that invaded HeLa cells under the control, LLAD (0.5 μmol/L, 1 μmol/L) and cisplatin (13.7 μmol/L) for 24 h (n = 3). LLAD channel: λ_{ex} = 405 nm, Em_{max} = 470 nm (411−500 nm); TMRE channel: λ_{ex} = 561 nm, Em_{max} = 575 nm (571−694 nm); Different groups analysis was performed using two-tailed unpaired Student's t-test, and the data were presented as mean ± SD. $P < 0.05$ was considered statistically significant.

with other drugs, LLAD showed unprecedented retention, persisting for 15 cell passages in HeLa cells after a single treatment. Furthermore, LLAD was characterized as a lysosomal target drug that induced long-term lysosomal damage and apoptosis in HeLa cells. This extended action in lysosomes not only enhanced its anticancer effects, but also suggested its potential to overcome drug resistance. We used this compound to examine its anticancer ability *in vitro* and *in vivo*. The results all showed that it has excellent efficacy as an anticancer agent in HeLa cells. *In vitro*, LLAD induced long-term lysosomal damage and apoptosis in

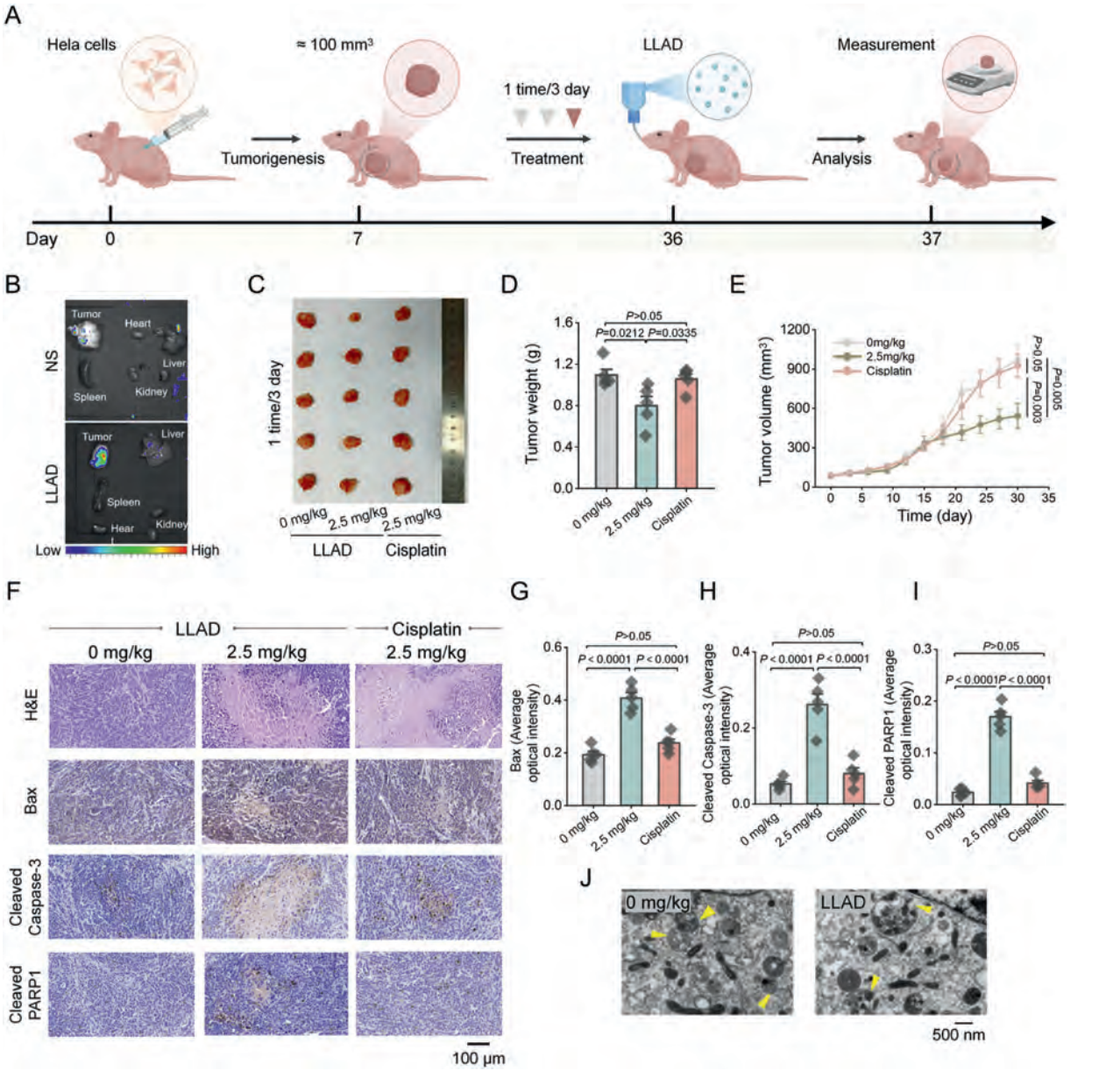

Figure 6 LLAD exhibited excellent long-term anticancer effect *in vivo*. (A) Schematic illustration of the treatment process for HeLa tumor-bearing BALB/c mice. (B) *Ex vivo* fluorescence imaging of the major organs at 24 h of NS or LLAD in mice. Normal Saline (NS) was used as a control group. (C) Representative images of tumors treated by different concentrations of LLAD (0 and 2.5 mg/kg) or cisplatin (2.5 mg/kg) every three days. (D) The weight of tumors treated with different concentrations of LLAD (0 and 2.5 mg/kg) or cisplatin (2.5 mg/kg) was administered every three days. (E) Changes in the tumor volume of mice treated with different concentrations of LLAD (0 and 2.5 mg/kg) or cisplatin (2.5 mg/kg) administrated every three days. (F) Representative hematoxylin and eosin staining, immunohistochemical staining with antibodies against Bax, Cleaved Caspase-3 and Cleaved PARP1 of tumors after different treatments. (G-I) Quantitative analysis the expression of Bax, Cleaved Caspased-3 and Cleaved PARP1 in tumor by immunohistochemistry. (J) TEM images of lysosomes in 2.5 mg/kg LLAD-treated and 0 mg/kg LLAD-treated tumor tissue administrated every three days. The yellow arrows indicate lysosomes. Analysis of different groups was performed using two-tailed unpaired Student's *t*-test, and the data are presented as the mean ± SD. A value of $P < 0.05$ was considered statistically significant.

HeLa cells, and inhibited their migration and invasion abilities. *In vivo*, LLAD not only exhibited its excellent performance as an anticancer drug in a dose-dependent manner, but also its significantly prolonged antitumor effect.

More broadly, our approach to design novel lysosomes targeting drugs may offer new perspectives within the area. This innovative approach not only prolongs the duration in tumor tissue, but also increases the drug efficiency and resistance. Furthermore, the capability of LLAD could be widely used in cancer treatment, promising to accelerate the discovery and application in organelle-targeting drugs.

In conclusion, we proposed an adhesive-bandage approach to design long-term lysosome-targeting anticancer small-molecule drugs, containing an SLC38A9-targeting covalently bound

moiety and an alkaline component. Using this approach, we synthesized LLAD, a fluorescent lysosome-targeting drug that induces sustained lysosomal damage and apoptosis in HeLa cells. LLAD demonstrated dose-dependent tumor growth inhibition and prolonged activity *in vivo*, marking it as a promising candidate for anticancer therapy. Our study paves the way for developing lysosomal targeting drugs against cancer and to overcome the drug resistance. It also accelerates the process of identifying organelle-targeting drugs and application in anticancer therapy.

4. Experimental

4.1. Synthesis and characterization of LLAD

*4.1.1. 4-Nitro-1H-indazole-3-carbaldehyde (**1**)*

Under the nitrogen stream, 2 mol/L HCl (42 mL) was added dropwise to the solution of $NaNO_2$(6.6 g, 0.0957 mol) in water (20 mL), and the reaction was stirred at 0 °C for 10 min. Then the solution of 4-nitroindole (2 g, 0.0123 mol) in DMF was added, and the mixture was stirred at 80 °C for 2 h. The mixture was quenched with water and extracted with ethyl acetate. The organic phase was combined and dried over anhydrous $MgSO_4$, filtered, and then concentrated. The residue was purified by flash chromatography to obtain compound **1** (0.847 g), yield 35.9%, HR-MS (ESI, *m/z*) Calcd. for $C_8H_6N_3O_3$, $[M+H]^+$ 192.0409. Found: 192.0399.

*4.1.2. 4-(4-Methylpiperazin-1-yl) benzene-1,2-diamine (**2**)*

Pd/C (0.266 g, 20%) was added to a solution of 1-(3,4-dinitrophenyl)-4-methylpiperazine (1.33 g, 5.00 mmol) in MeOH (100 mL) and the mixture stirred under H_2 for 3 h. The reaction mixture was filtered, and concentrated. The residue was purified by flash chromatography (20/1 to 10/1 petroleum CH_2Cl_2/MeOH) to give **2** (0.67 g), yield: 65.0%, HR-MS (ESI, *m/z*) Calcd. for $C_{11}H_{19}N_4$, $[M+H]^+$ 207.1610. Found: 207.1598.

*4.1.3. 3-(6-(4-Methylpiperazin-1-yl) -1H-benzo[d]imidazole-2-yl) -4-nitro-1H-indazole (**3**)*

Molecular sieve 4A was added to a solution of **1** (2.0 g, 0.0105 mol) and **2** (3.278 g, 0.0159 mol) in anhydrous DMF and the mixture was stirred at 25 °C for 4 h. The reaction mixture was quenched with water, and the mixture was extracted with ethyl acetate. The organic layer was washed with brine, dried over anhydrous Na_2SO_4, filtered, and concentrated. The residue was purified by flash chromatography (20/1 to 10/1 petroleum CH_2Cl_2/MeOH) to give **3** (1.26 g), yield: 32.0%, HR-MS (ESI, *m/z*) Calcd. for $C_{19}H_{20}N_7O_2$, $[M+H]^+$ 378.1678. Found: 378.1692.

*4.1.4. 3-3-(6-(4-Methylpiperazin-1-yl)-1H-benzo[d]imidazole-2-yl)-1H-indazol-4-amine (**4**)*

Pd/C (0.124 g, 10%) was added to a solution of **3** (1.26 g, 3.341 mmol) in MeOH (100 mL) and the mixture was stirred under nitrogen for 3 h. The reaction mixture was filtered, and concentrated. The residue was purified by flash chromatography (20/1 to 10/1 petroleum CH_2Cl_2/MeOH) to afford **4** (0.48 g), yield: 42.1%, m.p. 287.0−289.0 °C, ^{1}H NMR (500 MHz, DMSO-d_6) δ 13.19 (d, J = 19.5 Hz, 1H, −NH−), 12.66 (s, 1H, −NH−), 7.50 (d, J = 8.8 Hz, 2H, ArH), 7.09−7.03 (m, 1H. ArH), 6.97−6.90 (m, 1H, ArH), 6.61 (dd, J = 8.1, 2.9 Hz, 1H, ArH), 6.23 (t, J = 7.8 Hz, 1H, ArH), 3.23−3.04 (m, 8H, $-CH_2-$ × 4), 2.24 (s, 3H, $-CH_3$); HR-MS (ESI, *m/z*) Calcd. for $C_{19}H_{21}N_7$, $[M+H]^+$ 348.1937. Found: 348.1961.

4.1.5. N-(3-(6-(4-Methylpiperazin-1-yl) -1H-benzo[d] imidazole-2-yl)-1H-indazol-4-yl) acrylamide (LLAD)

Acryloyl chloride (58.66 mg, 0.648 mmol) was added to a solution of **4** (150 mg, 0.432 mmol) in anhydrous THF and the mixture was stirred at 25 °C for 1 h. The reaction mixture was concentrated and the residue was purified by flash chromatography (20/1 to 10/1 petroleum CH_2Cl_2/MeOH) to give LLAD (33.45 mg), as a white solid. Yield 19.3%, m.p. > 320 °C, ^{1}H NMR (500 MHz, DMSO-d_6) δ 14.28 (d, J = 20.7 Hz, 1H, −NH−), 14.06−13.94 (m, 1H, −NH−), 13.15 (d, J = 26.8 Hz, 1H, −NH−), 8.41 (d, J = 7.6 Hz, 1H, ArH), 7.65 (d, J = 8.8 Hz, 1H, ArH), 7.50−7.38 (m, 1H, ArH), 7.34 (dd, J = 8.3, 4.6 Hz, 1H, ArH), 7.09 (ddd, J = 20.6, 8.9, 2.2 Hz, 1H, ArH), 6.99 (d, J = 2.3 Hz, 1H, ArH), 6.80 (ddd, J = 16.9, 10.2, 3.1 Hz, 1H, =CH), 6.44 (dt, J = 17.1, 2.5 Hz, 1H, =CH), 6.11−5.96 (m, 1H, =CH−), 3.31−3.23 (m, 4H, $-CH_2-$ × 2), 2.77 (s, 4H, $-CH_2-$ × 2), 2.42 (s, 3H, $-CH_3$); ^{13}C NMR (126 MHz, DMSO-d_6) δ 164.14, 146.99, 143.26, 136.19, 135.51, 135.12, 133.11, 132.59, 128.55, 127.77, 118.62, 116.13, 114.68, 112.52, 110.42, 106.07, 98.16, 54.46, 49.20, 21.59; HR-MS (ESI, *m/z*) Calcd. for $C_{22}H_{23}N_7O$, $[M+H]^+$ 402.2037. Found: 402.2030.

4.2. Molecular docking

The SLC38A9 model was prepared using the Protein Preparation Wizard workflow in the Schrödinger 2005 platform (Schrödinger, LLC., NY, USA). The ligand was then docked into the arginine binding site using the Glide-based covalent docking module with default parameters. The docked pose with top-ranked Glide score was selected for further simulation.

4.3. Molecular dynamics

An MD simulation was performed for the complex of LLAD with SLC38A9 in the Schrödinger Desmond module according to the published method[61]. A truncated octahedral box of the TIP3P water model was constructed with Na or Cl as counter ions. Protein and ligand were charged with the OPLS 2005 force field. Prior to MD, energy minimisation was performed with a convergence threshold of 0.01 kcal/mol/Ã. Heating simulation was performed from 0 to 300 K using the Berendsen thermostat with a time step of 1 fs, and a total of 1200 ps of heating simulation was performed in the NVT ensemble. Equilibrium MD simulation was performed for 100 ns with a time step of 2 fs, using the NPT ensemble with a fixed temperature of 300 K and pressure of 1.01 bar. We chose a 10-ps recording interval, resulting in an MD trajectory of 2000 unique conformations of T24. Default settings were used for all other parameters. The analysis module in Desmond was used on the generated trajectory.

4.4. Cell culture

HeLa cells were cultured in Dulbecco's modified Eagle's medium (DMEM) supplemented with 10% FBS and penicillin−streptomycin (100 units/mL) in a 37 °C humidified incubator with 5% CO_2. A549 cells were cultured in Ham's F-12K supplement with 10% FBS and penicillin−streptomycin (100 units/mL) in a 37 °C humidified incubator with 5% CO_2.

4.5. Cytotoxicity assay

Cell cytotoxicity assay was measured using the Cell Counting Kit-8 (CCK-8) assay. HeLa cells were cultured in 96-well cell plate in an incubator for 24 h. Then, cells were treated with different concentrations of compounds for a suitable time. After treatment, 10 μL of CCK-8 solution was added to each well in the incubator for 2 h. Finally, we measured the absorbance of each well at 450 nm using a microplate reader.

4.6. Western blotting assay

Cells were cultured in a 6-well cell culture plate in a 37 °C humidified incubator for 24 h. Then, cells were treated with different kinds of compounds for an appropriate time. After treatment, cells were washed 3 times with cold PBS and harvested with cell scrapers, and lysed in cold lysis buffer containing an anti-protease mix. Protein concentration was measured by BCA protein assay (P0009, Beyotime, China). Cytoplasmic proteins were extracted from HeLa cells using the cytoplasmic and nuclear protein extraction kit (#P0028, Beyotime, China). Briefly, HeLa cells were lysed with buffer A. After 20 min of incubation, cytosolic extracts were collected after centrifugation at 12,000×*g* for 5 min. 30 μg protein was loaded onto SDS-polyacrylamide gels and then transferred to PVDF membranes. The membranes were blocked in 5% milk for 1 h at room temperature on a shaker and then incubated with antibodies at 4 °C overnight. After treatment, the membranes were washed 3 times and incubated with secondary antibodies in room temperature. The membranes were incubated with ECL substrate and imaged. Finally, the expression of the target bands was qualified using Image J software.

4.7. Cell staining and imaging

Cells were cultured in a glass-bottom microwell dish with 2 mL medium supplemented with 10% FBS and penicillin−streptomycin (100 units/mL) in an incubator for 24 h. Cells were then treated with different commercial probes and compounds for an appropriate time. After treatment, the cells were washed with PBS and phenol-free medium and then the cells were incubated in 1 mL phenol-free medium supplemented with 10% FBS. Confocal images were acquired using a confocal laser scanning microscope (Carl Zeiss, LSM 980, Germany). For SIM images, a super-resolution microscope (Carl Zeiss, Elyra 7 with Lattice SIM, Germany) with a 63 × oil objective was used.

4.8. Immunofluorescence

An appropriate number of cells were cultured in a glass-bottom microtitrer dish with 2 mL of complete medium in an incubator for 24 h. The cells were then treated with different concentrations of compounds for an appropriate period of time. After treatment, we removed the medium and fixed the cells with 4% paraformaldehyde for 20 min, then permeabilized with 0.1% Triton-PBS for 15 min. The cells were incubated with primary antibodies overnight on a shaker at 4 °C. The cells were then washed 3 times with Triton-PBS and incubated with secondary antibodies for 1 h on a shaker at room temperature. Finally, the cells were stained with DAPI and photographed using a confocal laser scanning microscope.

4.9. Transmission electron microscope (TEM)

Cells were treated with LLAD for 24 h and harvested with cell scrapers, fixed with 2.5% glutaraldehyde and placed at 4 °C for 24 h. Then washed with PBS 3 times for 15 min each time and fixed with 1% OsO_4 solution for 2 h. Then dehydrated at room temperature, resin embedded, polymerised and ultrathin sectioned. Sections were stained with uranium and observed by TEM in HT7800.

4.10. Surface plasmon resonance (SPR)

SPR was performed using a Biacore 1k + instrument. Preparation of A CM7 sensor chip, activate the surface of the chip through 1-(3-dimethylaminopropyl)-3-ethylcarbodiimide (EDC) and *N*-hydroxysuccinimide (NHC). The chip was subsequently immobilized with the amino coupling at a concentration of 50 μg/mL in sodium acetate. Various concentration of recombinant SLC38A9 was injected into the flow cell at a rate of 10 μL/min PBS-P+ (pH 7.4), and 5% dimethylsulfoxide (DMSO) running buffer. Use data analysis software to process the SPR response curves and calculate binding constants (K_D).

4.11. CETSA assay

Cellular target identification of LLAD was performed using CETSA as previously described[62]. Briefly, HeLa cells were incubated with LLAD at an appropriate concentration for 2 h, then treated and untreated cells were individually heated at different temperatures (49−74 °C) for 3 min, followed by cooling to room temperature. Cell lysates were obtained by freeze-thawing in liquid nitrogen for five cycles. Soluble proteins were centrifuged at 12,000×*g* for 30 min at 4 °C, and supernatants were detected by Western blot.

4.12. Transwell assay

The Transwell assay was used to measure the cell invasion ability of tumor cells *in vitro*. For cell invasion, Matrigel matrix was first mixed with medium to an appropriate concentration and added to the cell culture champers (8 mm pore size) for 1 h in a 37 °C incubator. Then 2×10^5 HeLa cells with serum-free medium were added to the upper chamber, also with different concentrations of LLAD (0, 0.5, and 1 μmol/L). Medium containing 10% FBS as chemoattractant was added to the lower chamber. After 24 h, the chambers were washed with PBS and fixed with 4% formaldehyde for 20 min. The cells were then washed with PBS and stained with crystal violet for 15 min. Finally, five fields of view were selected and photographed under an inverted microscope.

4.13. Detection of apoptosis by flow cytometry

Cells were cultured in 6-well cell plates with complete medium and penicillin−streptomycin (100 units/mL) in a 37 °C humidified incubator with 5% CO_2 for 24 h. Then cells were treated and untreated with different concentrations of LLAD for 24 h. After drug treatment, cells were trypsinized and centrifuged at 1000×*g* for 5 min. Cells were measured and centrifuged at 1200×*g* for 5 min in cold PBS. Annexin V-FITC and PI were added, the solutions were mixed well and the samples were incubated for 15 min in the dark at room temperature. Finally, cell fluorescence was detected by flow cytometry.

4.14. In vivo anti-cancer activity

All animal experiment procedures were conducted in conformity with institutional guidelines of the animal Ethics Committee of animal Experiment Center of Henan University of Chinese Medicine (Zhengzhou, China), approval number: DWLL202003251, and followed the national research council's guide for the care and use of laboratory animals.

Female BALB/c nude mice (4 weeks old) were housed under standard conditions. Typically, HeLa cells were diluted to 1×10^7/mL with serum-free medium and 200 μL of cell suspension was injected subcutaneously into the right arm of the mice on Day 0. Mice were randomly divided into 6 groups ($n = 6$) and orally administered LLAD (0, 2.5, 5.0 and 10.0 mg/kg/day) when the tumor volume reached approximately 100 mm^3. Mice in the solvent control group were treated with 1% DMSO. Cisplatin (2.5 mg/kg/day) was administered orally to the mice as a positive control group. Body weight and tumor volume were measured every three days. Solid tumor volume (V) was determined by measuring the longest diameter (A) and the shortest diameter (B) of the tumor using digital calipers and calculated as Eq. (1):

$$V = (A \times B^2)/2 \quad (1)$$

Mice were sacrificed on Day 23 and tumors and normal tissues were harvested for molecular analysis. We also treated tumor bearing mice with LLAD 2.5 mg/kg every three days and the same dose of cisplatin, and after sacrificing the mice on Day 32, tumor and normal tissues were harvested.

4.15. Data analysis

Each experiment was repeated three times independently with similar results. Statistical analysis was performed using Image J, GraphPad Prism 9.4.1 and Origin 2021. Normality and lognormality tests were performed to check for normal distribution. Data are presented as mean ± standard deviation (SD). Statistical comparison of results was performed using Student's t-test (Mann−Whitney) or ANOVA, $P < 0.05$ was considered statistically significant.

Acknowledgments

This work was financially supported by the National Natural Science Foundation of China (No. 82003566), Henan Excellent Youth Found (No. 242300421091, China) and Program for Innovative Research Team (in Science and Technology) in University of Henan Province (24IRTSTHN039, China).

Author contributions

Shulin Zhao and Qingjie Bai cultured cell. Guimin Xue and Juan Wang synthesized and characterized LLAD. Shulin Zhao, Qingjie Bai, Yangang Sun. and Yanling Mu performed confocal laser scanning microscopy. Xueqian Wang, Luyao Hu and Shulin Zhao collected all SIM super-resolution microscopy data. Yanling Mu, Yan Li and Zhiqiang Zhang conducted animal experiment. Shuai Lu conducted calculated work. Qixin Chen and Yanle Zhi conceived the project, designed the experiments, and wrote the manuscript with the help of all authors.

Conflicts of interest

The authors declare no conflicts of interest.

Appendix A. Supporting information

Supporting information to this article can be found online at https://doi.org/10.1016/j.apsb.2025.09.005.

References

1. Alu A, Han XJ, Ma XL, Wu M, Wei YQ, Wei XW. The role of lysosome in regulated necrosis. *Acta Pharm Sin B* 2020;**10**:1880−903.
2. Saftig P, Klumperman J. Lysosome biogenesis and lysosomal membrane proteins: trafficking meets function. *Nat Rev Mol Cell Biol* 2009;**10**:623−35.
3. Pellegrini FR, De Martino S, Fianco G, Ventura I, Valente D, Fiore M, et al. Blockage of autophagosome−lysosome fusion through SNAP29 *O*-GlcNAcylation promotes apoptosis *via* ROS production. *Autophagy* 2023;**19**:2078−93.
4. Ballabio A, Bonifacino JS. Lysosomes as dynamic regulators of cell and organismal homeostasis. *Nat Rev Mol Cell Biol* 2020;**21**:101−18.
5. Rebsamen M, Pochini L, Stasyk T, de Araújo ME, Galluccio M, Kandasamy RK, et al. SLC38A9 is a component of the lysosomal amino acid sensing machinery that controls mTORC1. *Nature* 2015;**519**:477−81.
6. Wang S, Tsun ZY, Wolfson RL, Shen K, Wyant GA, Plovanich ME, et al. Metabolism. Lysosomal amino acid transporter SLC38A9 signals arginine sufficiency to mTORC1. *Science* 2015;**347**:188−94.
7. Abu Remaileh M, Wyant GA, Kim C, Laqtom NN, Abbasi M, Chan SH, et al. Lysosomal metabolomics reveals V-ATPase- and mTOR-dependent regulation of amino acid efflux from lysosomes. *Science* 2017;**358**:807−13.
8. Banushi B, Joseph SR, Lum B, Lee JJ, Simpson F. Endocytosis in cancer and cancer therapy. *Nat Rev Cancer* 2023;**23**:450−73.
9. Zhitomirsky B, Assaraf YG. Lysosomes as mediators of drug resistance in cancer. *Drug Resist Updates* 2016;**24**:23−33.
10. Shi QZ, Shen QC, Liu YF, Shi Y, Huang WW, Wang X, et al. Increased glucose metabolism in TAMs fuels *O*-GlcNAcylation of lysosomal Cathepsin B to promote cancer metastasis and chemoresistance. *Cancer Cell* 2022;**40**:1207−22.e10.
11. Hraběta J, Belhajová M, Šubrtová H, Merlos Rodrigo MA, Heger Z, Eckschlager T. Drug sequestration in lysosomes as one of the mechanisms of chemoresistance of cancer cells and the possibilities of its inhibition. *Int J Mol Sci* 2020;**21**:4392.
12. Song Y, Zhang H, Wang X, Geng X, Sun Y, Liu J, et al. One stone, three birds: pH triggered transformation of aminopyronine and iminopyronine based lysosome targeting viscosity probe for cancer visualization. *Anal Chem* 2021;**93**:1786−91.
13. Kroemer G, Jäättelä M. Lysosomes and autophagy in cell death control. *Nat Rev Cancer* 2005;**5**:886−97.
14. Yang X, Wen Y, Liu S, Duan L, Liu T, Tong Z, et al. LCDR regulates the integrity of lysosomal membrane by hnRNP K-stabilized LAPTM5 transcript and promotes cell survival. *Proc Natl Acad Sci U S A* 2022;**119**:e2110428119.
15. He Y, Fan Y, Ahmadpoor X, Wang Y, Li ZA, Zhu W, et al. Targeting lysosomal quality control as a therapeutic strategy against aging and diseases. *Med Res Rev* 2024;**44**:2472−509.
16. Hu P, Li H, Sun W, Wang H, Yu X, Qing Y, et al. Cholesterol-associated lysosomal disorder triggers cell death of hematological malignancy: dynamic analysis on cytotoxic effects of LW-218. *Acta Pharm Sin B* 2021;**11**:3178−92.
17. Cao M, Luo X, Wu K, He X. Targeting lysosomes in human disease: from basic research to clinical applications. *Signal Transduct Targeted Ther* 2021;**6**:379.
18. Levy JMM, Towers CG, Thorburn A. Targeting autophagy in cancer. *Nat Rev Cancer* 2017;**17**:528−42.

19. Wiedmann RM, von Schwarzenberg K, Palamidessi A, Schreiner L, Kubisch R, Liebl J, et al. The V-ATPase-inhibitor archazolid abrogates tumor metastasis *via* inhibition of endocytic activation of the Rho-GTPase Rac1. *Cancer Res* 2012;**72**:5976−87.
20. Wang X, Zhao S, Fang G, Wang R, Lyu X, Shao X, et al. Lysosome passivation triggered by silver nanoparticles enhances subcellular-targeted drug therapy. *Nanoscale* 2024;**16**:8597−606.
21. Borkowska M, Siek M, Kolygina DV, Sobolev YI, Lach S, Kumar S, et al. Targeted crystallization of mixed-charge nanoparticles in lysosomes induces selective death of cancer cells. *Nat Nanotechnol* 2020; **15**:331−41.
22. LoRusso PM. Inhibition of the PI3K/AKT/mTOR pathway in solid tumors. *J Clin Oncol* 2016;**34**:3803−15.
23. Saxton RA, Sabatini DM. mTOR signaling in growth, metabolism, and disease. *Cell* 2017;**168**:960−76.
24. Wolin E, Mita A, Mahipal A, Meyer T, Bendell J, Nemunaitis J, et al. A phase 2 study of an oral mTORC1/mTORC2 kinase inhibitor (CC-223) for non-pancreatic neuroendocrine tumors with or without carcinoid symptoms. *PLoS One* 2019;**14**:e0221994.
25. Graham L, Banda K, Torres A, Carver BS, Chen Y, Pisano K, et al. A phase II study of the dual mTOR inhibitor MLN0128 in patients with metastatic castration resistant prostate cancer. *Invest N Drugs* 2018;**36**: 458−67.
26. Trybus W, Trybus E, Król T. Lysosomes as a target of anticancer therapy. *Int J Mol Sci* 2023;**24**:2176.
27. Gros F, Muller S. Pharmacological regulators of autophagy and their link with modulators of lupus disease. *Br J Pharmacol* 2014;**171**: 4337−59.
28. Varkouhi AK, Scholte M, Storm G, Haisma HJ. Endosomal escape pathways for delivery of biologicals. *J Control Release* 2011;**151**:220−8.
29. Tan JX, Finkel T. A phosphoinositide signalling pathway mediates rapid lysosomal repair. *Nature* 2022;**609**:815−21.
30. Ferreira PMP, Sousa RWR, Ferreira JRO, Militão GCG, Bezerra DP. Chloroquine and hydroxychloroquine in antitumor therapies based on autophagy-related mechanisms. *Pharmacol Res* 2021;**168**:105582.
31. Wang FMT, Liu DL, Cen YX, Deng SD, Zhang L, Lin GQ. High-throughput modular click chemistry synthesis of catechol derivatives as covalent inhibitors of SARS-CoV-2 $3CL^{pro}$. *Acta Materia Medica* 2024;**3**:328−44.
32. Xie X, Yu T, Li X, Zhang N, Foster LJ, Peng C, et al. Recent advances in targeting the "undruggable" proteins: from drug discovery to clinical trials. *Signal Transduct Targeted Ther* 2023;**8**:335.
33. Cai Y, Gui C, Samedov K, Su H, Gu X, Li S, et al. An acidic pH independent piperazine-TPE AIEgen as a unique bioprobe for lysosome tracing. *Chem Sci* 2017;**8**:7593−603.
34. Martinez Molina D, Nordlund P. The cellular thermal shift assay: a novel biophysical assay for *in situ* drug target engagement and mechanistic biomarker studies. *Annu Rev Pharmacol Toxicol* 2016;**56**: 141−61.
35. Liu Y, Guo Q, Yang H, Zhang XW, Feng N, Wang JK, et al. Allosteric regulation of IGF2BP1 as a novel strategy for the activation of tumor immune microenvironment. *ACS Cent Sci* 2022;**8**:1102−15.
36. Szwed A, Kim E, Jacinto E. Regulation and metabolic functions of mTORC1 and mTORC2. *Physiol Rev* 2021;**101**:1371−426.
37. Jindal AB, Bhide AR, Salave S, Rana D, Benival D. Long-acting parenteral drug delivery systems for the treatment of chronic diseases. *Adv Drug Deliv Rev* 2023;**198**:114862.
38. Hu M, Chen J, Liu S, Xu H. The acid gate in the lysosome. *Autophagy* 2023;**19**:1368−70.
39. Gan Z, Guo Y, Zhao M, Ye Y, Liao Y, Liu B, et al. Excitatory amino acid transporter supports inflammatory macrophage responses. *Sci Bull* 2024;**69**:2405−19.
40. Hu M, Li P, Wang C, Feng X, Geng Q, Chen W, et al. Parkinson's disease-risk protein TMEM175 is a proton-activated proton channel in lysosomes. *Cell* 2022;**185**:2292−308.e20.
41. Lakpa KL, Khan N, Afghah Z, Chen X, Geiger JD. Lysosomal stress response (LSR): physiological importance and pathological relevance. *J Neuroimmune Pharmacol* 2021;**16**:219−37.
42. Chen H, Fang G, Ren Y, Zou W, Ying K, Yang Z, et al. Super-resolution imaging for *in situ* monitoring sub-cellular micro-dynamics of small molecule drug. *Acta Pharm Sin B* 2024;**14**:1864−77.
43. Qi Z, Yang W, Xue B, Chen T, Lu X, Zhang R, et al. ROS-mediated lysosomal membrane permeabilization and autophagy inhibition regulate bleomycin-induced cellular senescence. *Autophagy* 2024;**20**:2000−16.
44. Yao RQ, Ren C, Xia ZF, Yao YM. Organelle-specific autophagy in inflammatory diseases: a potential therapeutic target underlying the quality control of multiple organelles. *Autophagy* 2021;**17**:385−401.
45. Eriksson I, Wäster P, Öllinger K. Restoration of lysosomal function after damage is accompanied by recycling of lysosomal membrane proteins. *Cell Death Dis* 2020;**11**:370.
46. Wang H, Jiang Y, Zhu M, Li H, Chen H, Wang H, et al. LW-213, a derivative of wogonin, triggers reticulophagy-mediated cell death in NSCLC *via* lysosomal damage combined with NPC1 inhibition. *Phytomedicine* 2024;**134**:155958.
47. Wang A, Chen C, Mei C, Liu S, Xiang C, Fang W, et al. Innate immune sensing of lysosomal dysfunction drives multiple lysosomal storage disorders. *Nat Cell Biol* 2024;**26**:219−34.
48. Wu Y, Zhang S, Gong X, Tam S, Xiao D, Liu S, et al. The epigenetic regulators and metabolic changes in ferroptosis-associated cancer progression. *Mol Cancer* 2020;**19**:39.
49. McCormack M, Eminowicz G, Gallardo D, Diez P, Farrelly L, Kent C, et al. Induction chemotherapy followed by standard chemoradiotherapy *versus* standard chemoradiotherapy alone in patients with locally advanced cervical cancer (GCIG INTERLACE): an international, multicentre, randomised phase 3 trial. *Lancet* 2024;**404**:1525−35.
50. Ren Y, Wu LL, Song W, Gao Y, Shao L, Lu Z, et al. Mitochondrial electron flow dynamics imaging for assessing mitochondrial quality and drug screening. *Adv Sci (Weinh)* 2025;**12**:e2410561.
51. Filomeni G, De Zio D, Cecconi F. Oxidative stress and autophagy: the clash between damage and metabolic needs. *Cell Death Differ* 2015; **22**:377−88.
52. Scherz-Shouval R, Elazar Z. Regulation of autophagy by ROS: physiology and pathology. *Trends Biochem Sci* 2011;**36**:30−8.
53. Gao Y, Bai Q, Ren Y, Shao X, Zhang M, Wu L, et al. A small-molecule drug for the self-checking of mitophagy. *Angew Chem Int Ed Engl* 2025;**64**:e202421269.
54. Chen Y, Yang Z, Wang S, Ma Q, Li L, Wu X, et al. Boosting ROS-mediated lysosomal membrane permeabilization for cancer ferroptosis therapy. *Adv Healthcare Mater* 2023;**12**:e2202150.
55. Liu X, Yuan Z, Luo L, Wang T, Zhao F, Zhang J, et al. Protective role of fruits of Rosa odorata var. gigantea against WIRS-induced gastric mucosal injury in rats by modulating pathway related to inflammation, oxidative stress and apoptosis. *Chin Herb Med* 2024;**16**:263−73.
56. Zhang Z, Hou L, Liu D, Luan S, Huang M, Zhao L. Directly targeting BAX for drug discovery: therapeutic opportunities and challenges. *Acta Pharm Sin B* 2024;**14**:2378−401.
57. Lu Z, Ren Y, Yang L, Jia A, Hu Y, Zhao Y, et al. Inhibiting autophagy enhances sulforaphane-induced apoptosis *via* targeting NRF2 in esophageal squamous cell carcinoma. *Acta Pharm Sin B* 2021;**11**: 1246−60.
58. Chu YJ, Xu QH, Zhou XD, Nie QY, Yao XJ, Fang JG, et al. Pristimerin inhibits thioredoxin reductase in the treatment of non-small cell lung cancer. *Acta Materia Medica* 2024;**3**:239−53.
59. Terman A, Gustafsson B, Brunk UT. The lysosomal−mitochondrial axis theory of postmitotic aging and cell death. *Chem Biol Interact* 2006;**163**:29−37.
60. Chen Y, Chen S, Chen K, Ji L, Cui S. Magnolol and 5-fluorouracil synergy inhibition of metastasis of cervical cancer cells by targeting PI3K/AKT/mTOR and EMT pathways. *Chin Herb Med* 2024;**16**:94−105.
61. Bao J, Liu H, Zhi Y, Yang W, Zhang J, Lu T, et al. Discovery of benzo [*d*]oxazole derivatives as the potent type-I FLT3-ITD inhibitors. *Bioorg Chem* 2020;**94**:103248.
62. Zhou X, Zhao S, Liu T, Yao L, Zhao M, Ye X, et al. Schisandrol a protects AGEs-induced neuronal cells death by allosterically targeting ATP6V0d1 subunit of V-ATPase. *Acta Pharm Sin B* 2022;**12**: 3843−60.